OPEN ACCESS Freely available online

IJCMB
International Journal of Clinical Medicine and Bioengineering

ISSN 2737-534X
Volume 4, Issue 3
https://ijcmb.iikii.com.sg
International Journal of Clinical Medicine and Bioengineering

Article

Porous Hydroxyapatite Bioscaffolds via Hybrid FDM-DLP 3D Printing with Porogen Engineering

Yu-Sheng Tseng [1, †], Wei-Hsi Chang [1, 2, 3,†], Yu-Jui Cheng [1], Chih-Kuang Wang [4] and Wen-Fan Chen [2,*]

[1] Institute of Medical Science and Technology, National Sun Yat-sen University, Kaohsiung 80424, Taiwan; johnson760515@gmail.com (Y.-S. Tseng); array90343@gmail.com (Y.-J. Cheng)
[2] Department of Emergency Medicine, Kaohsiung Armed Forces General Hospital, Kaohsiung 80284, Taiwan; wishviva@gmail.com
[3] Department of Emergency Medicine, Tri-Service General Hospital, National Defense Medical Center, Taipei 11490, Taiwan
[4] Department of Medicinal and Applied Chemistry, Kaohsiung Medical University, Kaohsiung, 80708 Taiwan; ckwang@kmu.edu.tw
* Correspondence: sallychen@imst.nsysu.edu.tw
† These authors contribute equally.

Received: Feb 03, 2024; **Revised:** Jun 17, 2024; **Accepted:** Jun 24, 2024; **Published:** July 19, 2024

Abstract: Porous hydroxyapatite (HA) bioscaffolds were successfully fabricated using a hybrid 3D printing approach that integrates fused deposition modeling (FDM) and digital light processing (DLP) technologies, with porogen additions ranging from 10 to 30%. HA was used as the primary scaffold material, while Pluronic F-127 (PF-127) served as the binder. To enhance porosity, NaCl, $NaHCO_3$, and PF-127 were incorporated as porogens. The results demonstrated that NaCl was inappropriate as a porogen, as it caused a complete fracture of the bioscaffolds after sintering. Similarly, $NaHCO_3$ altered the crystalline structure and reduced structural stability. In contrast, PF-127 effectively enhanced porosity and maintained scaffold integrity when added at concentrations up to 30%. Porosity analysis results revealed that bioscaffolds containing PF-127 exhibited a total porosity ranging from 46.90 to 64.79%, while hardness decreased from 1.69 GPa (without porogen) to 0.47 GPa at 20% PF-127. Degradation studies in simulated body fluid (SBF) showed that bioscaffolds without porogens exhibited a steady weight increase due to apatite deposition. However, bioscaffolds containing PF-127 exhibited weight fluctuations, resulting from an increased degradation rate balanced by apatite formation on the scaffold surface. The low degradation rate and well-developed porous structure of the fabricated HA bioscaffolds make them promising candidates for drug delivery applications.

Keywords: Bioceramic, Hydroxyapatite, Porogen, 3D printing, FDM, DLP

1. Introduction

Bone is a vital structural component of the human body, providing both mechanical support and functional protection. However, bone defects caused by trauma, tumor resection, congenital disorders, and degenerative diseases are common in clinical practice. If these defects fail to heal within a certain timeframe, they can lead to severe functional impairment, significantly impacting a patient's quality of life. Traditional treatment options include autografts [1], allografts [1–3], and synthetic bone substitutes [1], each of which presents specific limitations. Autografts require additional surgical procedures, allografts pose risks of immune rejection and disease transmission, and synthetic materials often fail to fully replicate the complex structure and biological function of natural bone tissue. Consequently, the search for an ideal bone replacement material has become a key focus in bone tissue engineering.

An ideal bone substitute closely resembles natural bone in terms of mechanical properties, biocompatibility, degradability, and osteogenic potential. Traditional synthetic bone materials, such as hydroxyapatite (HA) [4,5] and tricalcium phosphate (TCP) [6–8], have been extensively studied due to their chemical similarity to human bone. However, achieving a balance between mechanical strength and biocompatibility remains a significant challenge. Furthermore, the three-dimensional architecture of the scaffold plays a crucial role in facilitating cell attachment, proliferation, and bone tissue regeneration. With the rapid advancement of 3D printing technology, its application in bone tissue engineering has gained considerable attention. 3D printing enables the precise fabrication of biomimetic scaffolds with patient-specific and geometrically complex architectures, offering a promising solution for bone defect repair. Compared with conventional manufacturing techniques, 3D printing allows for customized scaffold designs based on patient-specific bone defects while precisely controlling geometry, pore size, and pore distribution to better mimic the microstructure and

mechanical properties of natural bone [9]. Additionally, 3D-printed scaffolds can be integrated with bioactive materials and cells to promote bone regeneration and functional restoration. Despite significant progress in 3D-printed bioceramic scaffolds [10–12], several challenges remain. For instance, fused deposition molding (FDM) is cost-effective and simple but lacks precision and mechanical strength, making it inappropriate for scaffolds with intricate architectures or high-load applications.

In contrast, digital light processing (DLP) technology offers high-resolution fabrication in a short period. However, concerns about biocompatibility arise due to residual photosensitizers on the scaffold surface. To address these challenges, we have pioneered an innovative hybrid 3D printing strategy that synergizes FDM and DLP technologies to fabricate high-strength hydroxyapatite (HA) bioscaffolds, as previously reported in our study [13]. In this approach, HA was utilized as the primary bioceramic material, while Pluronic F-127 (PF-127) functioned as the binder. A well-dispersed bioceramic slurry, composed of HA and PF-127, was cast into outer molds fabricated via FDM printing. Unlike conventional subtractive manufacturing, the FDM technique offers a rapid and flexible way to adjust the outer mold's dimensions and design, ensuring compatibility with different equipment specifications for subsequent vacuum centrifugal defoaming, which enhances the scaffold's density. Furthermore, the resin-based outer molds produced by FDM exhibit sufficient structural integrity to endure the vacuum centrifugal defoaming process, eliminating the necessity for costly metal molds and thus significantly reducing fabrication expenses. Concurrently, a high-resolution DLP 3D printer was used to produce precisely structured struts, which were strategically embedded into the slurry to define the intended channel architecture. The DLP printing technique enables scalable and economical production, with tunable channel dimensions and porosity achieved by modifying the strut design parameters, such as spacing and diameter. Importantly, the resin material utilized in DLP does not become part of the bioscaffold itself; it merely contacts the surface of the sample and is eliminated during the sintering process, ensuring complete biocompatibility. After the placement of the struts, vacuum centrifugal defoaming was employed to expel air bubbles, even at the nanoscale, thereby markedly improving the homogeneity and density of the HA slurry. This critical step contributes to the outstanding compressive strength exhibited by the bioscaffold. Ultimately, fully crystallized HA bioscaffolds with enhanced mechanical properties were achieved after drying and high-temperature sintering.

A porous bioscaffold with a well-defined three-dimensional structure provides a large surface area, a critical factor for cell adhesion, proliferation, and nutrient exchange [14]. Various strategies have been explored to enhance scaffold porosity, including gas foaming [15,16], phase separation [17], freeze-drying [18], and particulate leaching [19]. Among these, porogen addition remains the most widely used method due to its simplicity, high efficiency, and versatility in selecting different porogen. However, not all porogens are appropriate for bioscaffold fabrication. Therefore, in this study, the effects of different porogens (NaCl, $NaHCO_3$, and PF-127) were investigated to identify the most suitable type and optimize its concentration for fabricating high-performance HA bioscaffolds. By integrating four key technologies: FDM, DLP, vacuum centrifugal defoaming, and porogen-assisted fabrication, this approach enables the production of high-strength bioscaffolds with a well-balanced porous structure, making them promising for advanced bone tissue engineering applications.

2. Materials and Methods

In this study, HA (Alfa Aesar, USA) was used as the primary raw material, while PF-127 (Sigma-Aldrich, USA) served as the binder for bioscaffold fabrication. The outer mold was produced using PLA resin (MIN-YAU, Taiwan), whereas the struts forming the penetrating channels within the bioscaffolds were printed using Insta Resin Grey (Capybara Robot, Taiwan), DLP photosensitive resin. To facilitate demolding, petroleum jelly (Chan Guare Industry, Taiwan) and lubricant (7717-GW, Taiwan Taisheng, Taiwan) were applied as release agents to the surfaces of both the outer molds and struts. To enhance the porosity of the bioscaffolds, three types of porogens: PF-127, $NaHCO_3$ (Sigma-Aldrich, USA), and NaCl (Sigma-Aldrich, USA). These porogens were sieved to ensure a particle size of less than 200 μm. The detailed preparation process for the fused deposition modeling (FDM)-printed plastic outer mold and the DLP-printed struts was described in our previous study [13]. In this study, the bioscaffold structure was designed based on the optimized parameters from the previous study in which an optimal strut diameter of 800 μm and a designed porosity of 10% were employed. These parameters served as the foundation for investigating the effects of varying porogen types and concentrations. To fabricate bioscaffolds with varying porosity levels, the three porogens were added individually to the ceramic slurry at concentrations of 10, 20, and 30 wt% before mixing and shaping. A pure HA bioscaffold without porogen addition was used as the control group and designated 800_{10}.

Before infusing the ceramic slurry, a layer of lubricant was applied to the inner walls of the outer mold to prevent adhesion during drying and demolding. Meanwhile, the DLP-printed struts were dip-coated with petroleum jelly and lubricant at 60°C, forming a double-layer release agent coating to facilitate their subsequent removal. The overall bioscaffold fabrication process followed a similar preparation method described in a previous study [13], and a detailed flowchart is presented in Figure 1. To prepare the binder for ceramic slurry mixing, PF-127 was dissolved in deionized (DI) water at a 1:4 ratio. The mixture was placed in a sealed glass vial and stored at 5°C for 72 h until complete dissolution. Subsequently, hydroxyapatite (HA) powder was mixed

with the PF-127 solution at a 1:1.2 ratio and kept at 5°C for 15 min to obtain a homogeneous HA slurry. For the preparation of HA slurry containing porogens, a portion of the HA powder was replaced with porogens at concentrations of 10 wt.%, 20 wt.%, and 30 wt.%. A planetary centrifugal mixer (MV-300S, CGT Technology, Taiwan) was used to homogenize the slurry at 1500 and 1200 rpm for 120 s. The prepared slurry was then transferred into a 10 ml syringe for subsequent mold filling. For bioscaffold formation, 1 g of slurry was injected into the mold and subjected to additional mixing in a planetary centrifugal mixer (1500 and 1200 rpm, and 120 s) to ensure uniform distribution at the mold base while minimizing air bubbles. The DLP-printed struts were then vertically inserted into the mold, which was subsequently sealed and stored at 5°C for 30 min. To further eliminate trapped air, vacuum defoaming was performed using the planetary centrifugal mixer under the same conditions. Notably, this centrifugal vacuum defoaming process removes trapped air and utilizes the centrifugal force to enhance the density of the bioscaffold, thereby improving its mechanical strength. The entire mold, including the embedded struts and slurry, was then sealed and stored at 5°C for an additional 60 min before being transferred to a humidity-proof drying chamber for 48 h. Following the drying process, a CO_2 laser cutter (65% laser power, 3 mm/s cutting speed) was used to remove the bottom portion of the DLP struts. The samples were then placed in an oven at 90°C for 60 min, a step designed to soften the DLP struts embedded within the HA ceramic structure, facilitating their subsequent removal. To refine the surface finish, the HA ceramic samples were polished using 1000-grit sandpaper before undergoing sintering. During sintering, the temperature was gradually increased to 450°C at a rate of 5°C/min and held for 2 h to remove polymers, moisture, impurities, and porogens from the ceramic bioscaffold. The temperature was then ramped up to 1200°C at a rate of 10°C/min and maintained for 2 h to eliminate residual porogens and densify the ceramic matrix, ultimately forming the final HA bioscaffold.

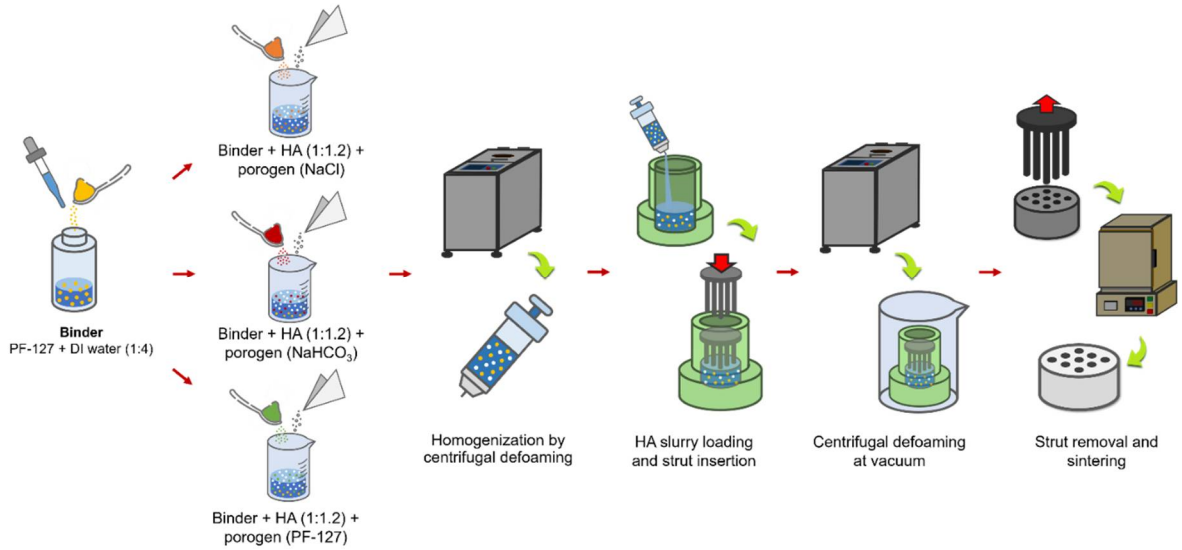

Figure 1. Flowchart of bioscaffold fabrication in this study.

For sample characterization, the weight of each sample was measured using an analytical balance (AS 220.R2 PLUS, Radwag, Poland). The dimensions of the samples were determined with a Vernier caliper and an optical microscope (IX73P1F, Olympus, Japan). To assess phase composition and confirm the complete removal of adhesives, porogen, and impurities, the sintered bioscaffolds were analyzed by X-ray diffraction (XRD, D2 Phaser, Bruker, USA). The density of the bioscaffolds was evaluated by using Archimedes' method [13] in deionized water. For mechanical strength analysis, the hardness of the bioscaffolds was measured using a Vickers hardness tester (FM-810, Future-Tech, Japan). A load of 0.5 kg was applied for each measurement, with five indentations taken at different positions on each sample. Each indentation was held for 10 s, and the final hardness value was reported as the average of the five measurements. Degradation testing was conducted by immersing the sintered bioscaffolds in a simulated body fluid (SBF) prepared at 36.5 ± 0.5°C, following the formula developed by Kokubo *et al.* [20]. Each sample was submerged in 45 ml of SBF solution at 37°C for 7, 14, 21, and 28 days. After the designated immersion periods, the samples were dried at 60°C for 24 h before being weighed. The weight loss of the samples was calculated as a percentage using the following formula:

$$W_L = [(W_F - W_0) / W_0] \times 100\% \quad (1)$$

where W_L represents the weight loss after SBF immersion, W_F is the final weight of the sample post-immersion, and W_0 is the initial weight of the sample before immersion.

3. Results and Discussion

The photographs of dried and sintered HA bioscaffolds with and without porogens are presented in Figure 2, while the dimensions of the dried and sintered samples and their shrinkage rates are summarized in Tables 1 and 2, respectively. Figures 2(a1) and (a2) show HA bioscaffolds without a porogen after drying and sintering, serving as the control group (designated as sample 800_{10}) to evaluate the effects of porogen addition. When NaCl was used as a porogen, part of NaCl dissolved in the binder during the slurry mixing process due to its solubility in water. This altered the overall composition of the raw materials (HA + NaCl + PF-127), leading to structural instability. As a result, a large number of cracks formed on the surface of the dried samples, resulting in fragile structures (Figure 2(b1)). After sintering, these samples fractured completely, making them unsuitable for further use (Figure 2(b2)).

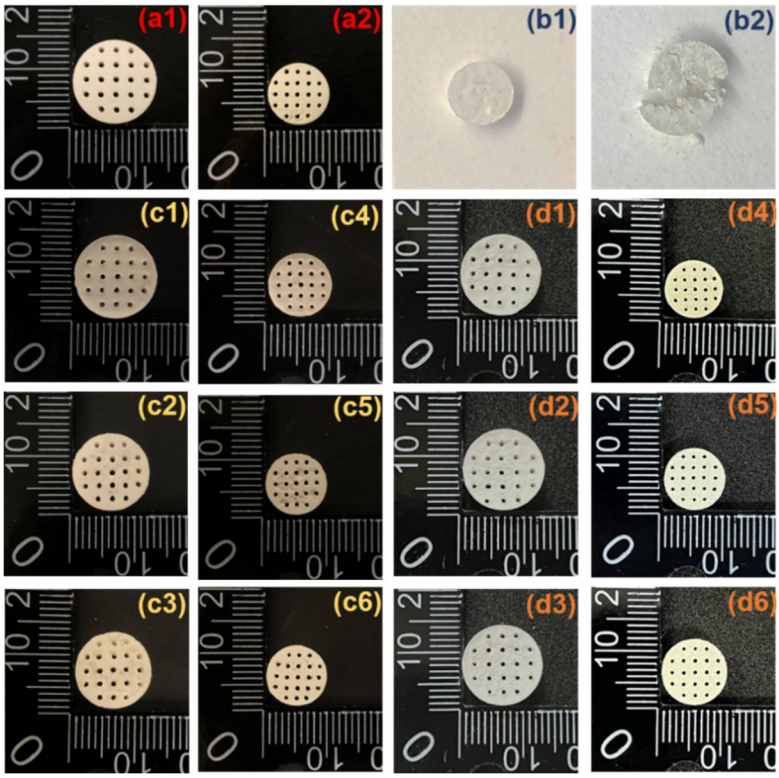

Figure 2. Photographs of dried and sintered samples with different porogens. After drying: (**a1**) 800_{10}, (**b1**) NaCl 10%, (**c1**)-(**c3**) PF-127 10-30%, and (**d1**)–(**d3**) $NaHCO_3$ 10-30%. After sintering: (**a2**) 800_{10}, (**b2**) NaCl 10%, (**c4**)–(**c6**) PF-127 10-30%, and (**d4**)–(**d6**) $NaHCO_3$ 10–30%.

Table 1. Dimensions of HA bioscaffolds with and without porogens after drying and sintering.

Sample	After Drying				After Sintering			
	Weight (g)	Ø (mm)	Pore Size (µm)	Designed Porosity (P_d) (%)	Weight (g)	Ø (mm)	Pore Size (µm)	Designed Porosity (P_d) (%)
800_{10}	0.509	12.56	851	9.6	0.376	9.32	645	10.1
$PF127_{10\%}$	0.556	12.23	779	8.52	0.358	9.62	611	8.5
$PF127_{20\%}$	0.511	11.49	832	11.01	0.287	9.36	635	9.97
$PF127_{30\%}$	0.576	11.42	834	11.18	0.271	9.47	671	10.5
$NaHCO3_{10\%}$	0.542	12.37	795	8.67	0.374	9.12	715	12.91
$NaHCO3_{20\%}$	0.54	12.32	757	7.95	0.338	9.77	776	13.26

$NaHCO3_{30\%}$	0.536	12.44	800	8.69	0.328	9.83	782	13.3

Table 2. Dimensional change (%) in HA bioscaffolds with and without porogens after drying and sintering.

Sample	After Drying				After Sintering			
	Weight (g)	Ø (mm)	Pore Size (μm)	Designed Porosity (P_d) (%)	Weight (g)	Ø (mm)	Pore Size (μm)	Designed Porosity (P_d) (%)
800_{10}	-49.1	-10.2	6.3	-0.4	-62.4	-33.4	-19.3	0.1
$PF127_{10\%}$	-44.4	-12.6	-2.6	-1.5	-64.2	-31.2	-23.5	-1.5
$PF127_{20\%}$	-48.9	-17.9	4	1.1	-71.3	-33.1	-20.6	-0.03
$PF127_{30\%}$	-42.4	-18.4	4.1	1.2	-72.9	-32.3	-16.1	0.5
$NaHCO3_{10\%}$	-45.8	-11.6	-0.6	-1.33	-62.6	-34.8	-10.6	2.91
$NaHCO3_{20\%}$	-46	-12	-5.3	-2.05	-66.2	-30.2	-3	3.26
$NaHCO3_{30\%}$	-46.4	-11.1	0	-1.31	-67.2	-29.7	-2.2	3.3

During the initial drying process, the samples containing PF-127 as a porogen exhibited a nearly translucent appearance. As shown in Figure 2(c1), when 10% PF-127 was added, the sample dimensions remained relatively unchanged. However, as the PF-127 content increased, the bioscaffold diameter slightly decreased. Although the pore diameter did not change significantly, the reduction in overall sample size resulted in a higher porosity than the original designed porosity (10%). When the PF-127 concentration reached 30%, the bioscaffold remained soft and could not fully harden after drying, and the pores became irregularly shaped (Figure 2(c3)). These findings suggest that excessive PF-127 leads to structural instability, even after water evaporation, compromising its effectiveness as a porogen. Therefore, to ensure bioscaffold stability, it is recommended that the PF-127 content must not exceed 30%. After sintering, the results confirmed that the addition of PF-127 as the porogen significantly affected both the weight and dimensional changes of the bioscaffolds. As PF-127 content increased, the weight of the sintered samples decreased considerably, as the porogen was fully removed during sintering. Additionally, the pore size increased with higher PF-127 concentrations after sintering, which in turn enhanced the designed porosity.

The drying results for $NaHCO_3$ showed that its use as a porogen led to more pronounced pore shrinkage (compared with 800_{10} samples without porogen) than that observed in PF-127-containing samples. This shrinkage resulted in a lower designed porosity, along with surface and bottom irregularities, as shown in Figure 3. However, after sintering, the pore size in $NaHCO_3$-containing samples did not exhibit significant shrinkage, making their final designed porosity even larger compared to other porogen types. Furthermore, the bioscaffold structure became fragile, weak, and prone to pulverization after sintering. During fabrication, bioscaffolds with $NaHCO_3$ as the porogen were more prone to damage, exhibiting higher instability and failure rates.

Based on the overall results, bioscaffold samples with PF-127 concentrations ranging from 10 to 30% exhibited designed pore sizes between 611 and 671 μm after sintering. This pore size range is favorable for bone cell infiltration and adhesion, facilitating effective bone regeneration [13]. Among these, PF-127 at 10 and 20% demonstrated an optimal pore-forming ability, successfully increasing porosity while maintaining structural integrity. However, at a 30% concentration, the samples failed to solidify properly and exhibited irregular shapes after the drying process, indicating a loss of mechanical stability. Therefore, subsequent experiments were carried out using only 10 and 20% PF-127. $NaHCO_3$ significantly affected the pore structure and mechanical strength of the bioscaffolds. At higher concentrations, the strength of the bioscaffolds decreased significantly, and pore shrinkage and structural fragility were observed. NaCl was found to be inappropriate as a porogen, as it induced cracks during drying and completely disintegrated after sintering.

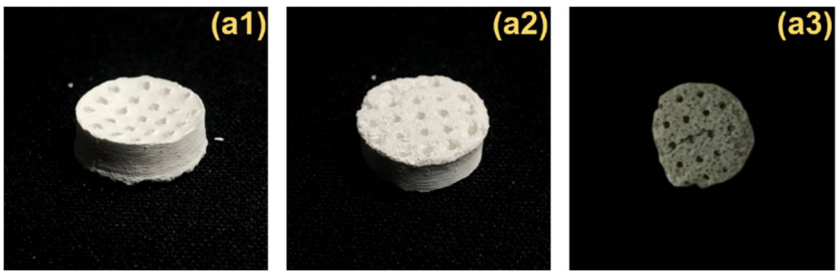

Figure 3. Photographs of HA bioscaffold with 30% $NaHCO_3$: (**a1**), (**a2**) sample after drying, and (**a3**) sample after sintering.

Figure 4 illustrates the effects of different porogens and their varying concentrations on the crystalline structure of HA bioscaffolds. As demonstrated in the previous study [13], the bioscaffold without any porogen consisted purely of HA. In the current study, XRD analysis confirmed that samples containing PF-127 as a porogen (Figures 4(d), 4(e), and 4(f)) exhibited diffraction patterns identical to standard HA, without the presence of secondary peaks. This indicates that PF-127 was completely decomposed during sintering and did not interfere with the HA crystalline structure. In contrast, bioscaffolds incorporating $NaHCO_3$ as a porogen (Figures 4(a), 4(b), and 4(c)) displayed distinctly different results. The addition of $NaHCO_3$ led to the appearance of new secondary peaks, with their intensity increasing as the $NaHCO_3$ content rose. This suggests that the sintering process induced the formation of new crystalline phases. Furthermore, the intensity of the characteristic HA peaks significantly decreased with increasing $NaHCO_3$ concentration, and a noticeable shift in some HA peaks was observed, further confirming that the crystalline structure was altered. These results indicate that $NaHCO_3$ chemically reacted with HA at high temperatures, leading to structural modifications. Overall, this study confirms that PF-127 was the most appropriate porogen, as it effectively enhanced porosity without disrupting the HA crystalline structure.

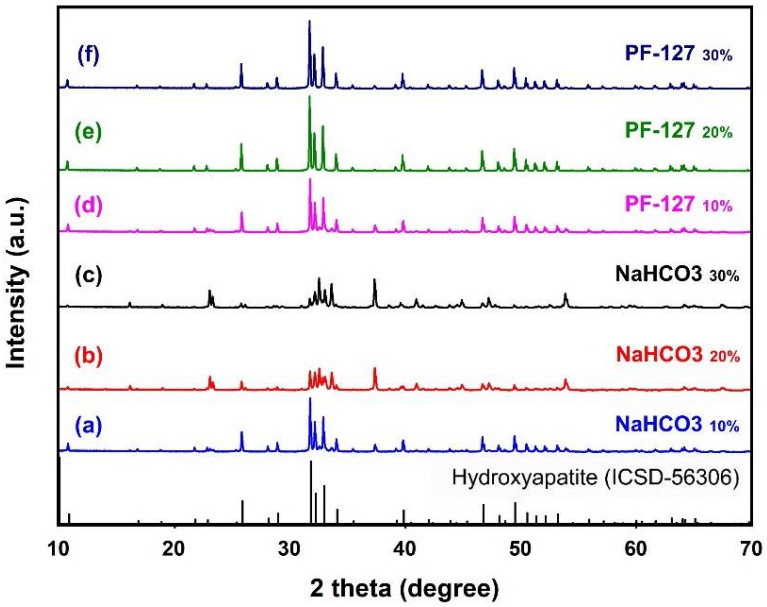

Figure 4. XRD spectra of sintered HA bioscaffolds with different porogens: (a) 10% $NaHCO_3$, (b) 20% $NaHCO_3$, (c) 30% $NaHCO_3$, (d) 10% PF-127, (e) 20% PF-127, and (f) 30% PF-127.

Table 3 presents the analysis of density and porosity in the bioscaffolds after sintering. The results indicate that the addition of PF-127 as a porogen significantly increased the open porosity (P_o), with a positive correlation between porosity and the porogen concentration. However, when the porogen content reached 30%, the increase in P_o became less pronounced. This phenomenon is attributed to the fact that at a 30% porogen concentration, the bioscaffold failed to fully dry and harden during fabrication, leading to poor structural integrity and shape retention. Therefore, to maintain the desired shaping quality and structural stability, the porogen content must not exceed 30%. The total porosity (P_t) is defined as the sum of open porosity (P_o), closed porosity (P_c), and designed porosity (P_d), with detailed definitions and calculation methods provided in our previous study [13]. P_t increased from 33.35 to 64.79% as the porogen content increased. The fabrication process enables precise control over pore size and porosity by adjusting the porogen ratio, thereby allowing the formation of a well-distributed network of small pores within the bioscaffolds. These small pores play a crucial role in enhancing the bioscaffold's surface area, which in turn promotes interaction with the physiological environment, accelerates degradation rates, and enhances the scaffold's potential as a drug carrier. Notably, when the PF-127 concentration was increased from 20 to 30%, the total porosity (P_t) exhibited only a slight increase of 4%. Given this marginal improvement, it is recommended to keep the PF-127 content at 20% or lower to optimize scaffold properties while maintaining structural integrity.

Table 3. Density analysis of sintered bioscaffolds with the PF127 porogen.

Sample	D_b (g/cm^3)	D_a (g/cm^3)	P_o (%)	P_c (%)	P_d (%)	$P_o + P_c$ (%)	P_t (%)
800_{10}	2.34	3.05	20.65	2.3	10.4	22.95	33.35

PF127$_{10\%}$	1.86	3.08	35.55	1.35	10.00	36.90	46.90
PF127$_{20\%}$	1.38	3.10	49.92	0.74	9.99	50.65	60.65
PF127$_{30\%}$	1.25	3.12	53.54	0.34	10.91	53.88	64.79

Figure 5(a) illustrates the hardness of the sintered HA bioscaffolds. The results indicate that the hardness significantly decreased with the addition of PF-127 porogen, primarily due to the increase in porosity. As porosity increases, the overall structural density decreases, leading to a reduction in mechanical strength. Figure 5(b) presents the weight loss of the bioscaffolds after immersion in SBF for 0, 7, 14, 21, and 28 days. The results show that weight fluctuations for all bioscaffolds remained within ±1%, which can be attributed to a balance between bioscaffold degradation (weight loss) and apatite formation due to the reaction between the bioscaffold and the SBF solution (weight gain). The 800_{10} bioscaffold (control group) exhibited a steady weight increase after immersion. However, the bioscaffolds with 10 and 20% porogen showed slightly different weight variations. This discrepancy can be explained by the absence of small pores in the 800_{10} bioscaffold, which resulted in a slower degradation rate. Consequently, the rate of apatite formation exceeded the degradation rate, leading to a slight increase in weight. When 10% PF-127 porogen was added, the increased surface area led to an accelerated degradation rate, which surpassed the apatite formation rate, resulting in a slight weight decrease. However, as PF-127 porogen content increased to 20%, the overall weight of the bioscaffolds began to increase again. This suggests that although higher porosity accelerates degradation, it also enhances apatite formation by increasing the exposed surface area, ultimately influencing the overall weight trend.

Based on Table 3, the total porosity (P_t) of bioscaffold samples containing 0 to 30% PF-127 porogen ranged from 33.35 to 64.79%, which falls within the typical porosity range of human cancellous bone (30–95%). However, considering the instability of samples containing 30% PF-127, only those with 0–20% PF-127 were included in the analysis. Figure 5(c) illustrates a positive linear correlation between PF-127 concentration and P_t, with the corresponding equation as follows ($R^2 = 1$):

$$y = 1.365x + 33.317 \quad (2)$$

where y represents P_t (%), and x denotes the PF-127 porogen content (0–20 wt.%).

Additionally, Figure 5(c) demonstrates a negative linear correlation between PF-127 concentration and hardness, described by the following equation ($R^2 = 0.9928$):

$$y' = -0.061x + 1.66 \quad (3)$$

where y′ represents hardness (GPa), and x is the PF-127 porogen content (0–20 wt.%).

These findings provide a valuable reference for biomaterial developers, enabling them to fine-tune the PF-127 porogen concentration based on Figure 5(c) and Equations (2) and (3) to achieve the desired bioscaffold porosity and mechanical strength for specific applications. For instance, human cancellous bone can be categorized into two structural types depending on loading conditions [21]. In regions subjected to asymmetric loading conditions (e.g., spine, tibia, femur, and calcaneus), the trabecular structure tends to form asymmetric cells. In contrast, regions experiencing uniaxial loading (e.g., vertebrae and proximal tibial epiphysis) develop a columnar cell structure. Notably, under the same porosity level, asymmetric cells exhibit higher mechanical strength compared with columnar cells. As porosity decreased from 60 to 30%, the strength of asymmetric cells gradually increased from 2.6 times to 4.7 times that of columnar cells [13,21]. Therefore, when repairing asymmetric cell-dominated regions, a lower PF-127 porogen concentration (<10 wt.%) is recommended to reduce porosity and enhance the bioscaffold's mechanical strength. Conversely, for columnar cell-dominated regions, a higher PF-127 porogen concentration (≥10 wt.%) is preferable, as it increases porosity and facilitates faster bone cell infiltration.

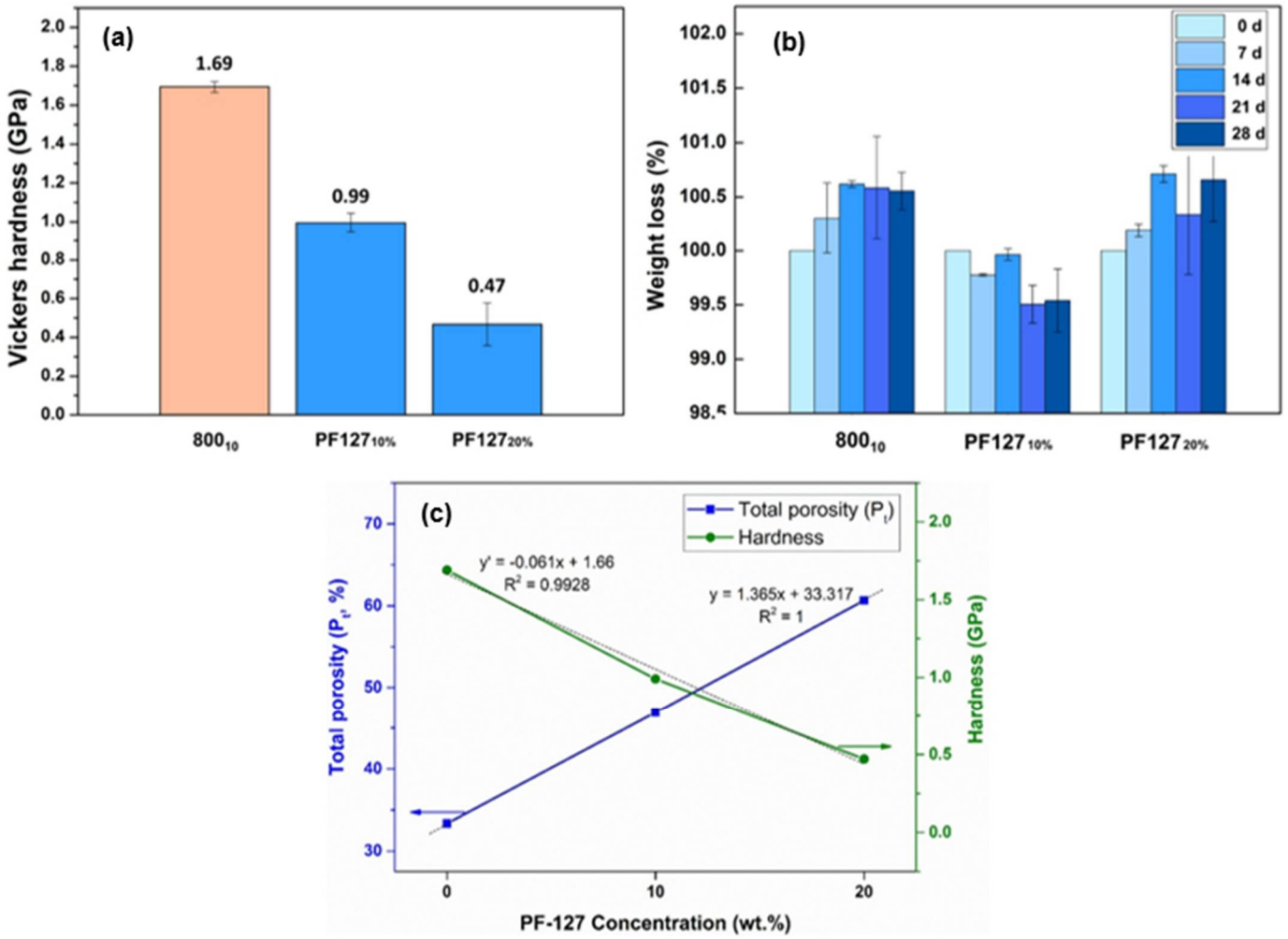

Figure 5. Relationship between PF-127 concentration and (**a**) hardness, (**b**) weight loss over time, and (**c**) total porosity and hardness of the sintered bioscaffolds.

4. Conclusions

In this study, porous hydroxyapatite (HA) bioscaffolds were successfully fabricated using a hybrid 3D printing approach that combined FDM and DLP technologies. HA, a bioceramic material with properties similar to human bone, was used as the primary scaffold material, while PF-127 served as the binder. To enhance porosity, NaCl, $NaHCO_3$, and additional PF-127 were individually incorporated as porogens to investigate their effects on scaffold structure and performance. The fabrication process involved preparing a ceramic slurry containing HA and porogen, which was then injected into an FDM-printed outer mold. After drying, the HA bioscaffold was extracted from the mold, separated from the DLP-printed struts, and sintered at 1200°C to achieve the final structure. The results demonstrated that NaCl was unsuitable as a porogen, as it caused a complete fracture of the sintered bioscaffolds. Although $NaHCO_3$ generated porous bioscaffolds, it induced crystalline phase alterations during sintering, leading to structural instability. In contrast, PF-127 proved to be the most effective porogen for enhancing porosity while maintaining scaffold integrity. However, its concentration must not exceed 30% and be preferably kept below 20%, as excessive amounts compromise scaffold formation. Porosity analysis using Archimedes' method revealed that the total porosity of PF-127-incorporated bioscaffolds increased to 46.90–64.79%, significantly improving pore configuration and functional adaptability for various biomedical applications. Mechanical testing indicated that the hardness of the bioscaffolds decreased from 1.69 GPa (without porogen) to 0.47 GPa when the PF-127 content reached 20%. Additionally, we analyzed the linear relationship between PF-127 porogen concentration (0–20 wt.%) and both total porosity and hardness, providing valuable guidance for selecting appropriate scaffold properties for different bone defect repair applications. Furthermore, degradation studies in simulated body fluid (SBF) revealed that bioscaffolds without porogen exhibited a steady weight increase due to apatite deposition, whereas those with PF-127 showed weight fluctuations caused by increased degradation rates and enhanced apatite formation on the scaffold surface. Overall, the HA

bioscaffolds fabricated in this study exhibited low degradability and a well-developed microporous structure as promising candidates for biomedical applications, including drug delivery systems. These findings provide a basis and a reference for optimizing scaffold fabrication techniques for future bone tissue engineering and regenerative medicine applications.

Author Contributions: conceptualization, Y.-S. Tseng and W.-F. Chen; methodology, Y.-S. Tseng, Y.-J. Cheng and W.-F. Chen; validation, Y.-S. Tseng and Y.-J. Cheng; formal analysis, Y.-J. Cheng; data curation, Y.-J. Cheng amd C.-K. Wang; writing—original draft preparation, W.-F. Chen; writing—review and editing, Y.-S. Tseng; visualization, Y.-J. Cheng and W.-H. Chang; supervision, W.-F. Chen.

Funding: This research was funded by National Science and Technology Council under contract NSTC 113-2636-E-110-002 - and Kaohsiung Armed Forces General Hospital Grant No. KAFGH_D_114072 and National Sun Yat-Sen University/Kaohsiung Medical University Grant No. 109KN004.

Data Availability Statement: The data of this study are available from the corresponding author upon reasonable request.

Acknowledgments: The authors acknowledge the Environmental Scanning Electron Microscope equipment provided by Joint Center for High Valued Instruments at National Sun Yat-Sen University.

Conflicts of Interest: The authors declare no conflict of interest.

References

1. Baldwin, P.; Li, D. J.; Auston, D. A.; Mir, H. S.; Yoon, R. S. & Koval, K. J. Autograft, allograft, and bone graft substitutes: Clinical evidence and indications for use in the setting of orthopaedic trauma surgery. *Journal of orthopaedic trauma* **2019**, *33*(4), 203–213.
2. Jeong, K. J.; Yang, E.; Jang, K.; Shim, K. M.; Bae, C. S.; Kim, S. E. & Kang, S. S. Successful clinical application of cancellous allografts with structural support for failed bone fracture healing in dogs. *in vivo* **2019**, *33*(6), 1813–1818.
3. Errani, C.; Ceruso, M.; Donati, D. M. & Manfrini, M. (2019). Microsurgical reconstruction with vascularized fibula and massive bone allograft for bone tumors. *European Journal of Orthopaedic Surgery & Traumatology* **2019**, *29*, 307–311.
4. Kattimani, V. S.; Kondaka, S. & Lingamaneni, K. P. (2016). Hydroxyapatite—Past, present, and future in bone regeneration. *Bone and Tissue Regeneration Insights* **2016**, *7*, BTRI-S36138.
5. Bal, Z.; Kaito, T.; Korkusuz, F. & Yoshikawa, H. (2020). Bone regeneration with hydroxyapatite-based biomaterials. *Emergent Materials* **2020**, *3*, 521–544.
6. Bohner, M.; Santoni, B.L.G. & Döbelin, N. (2020). β-tricalcium phosphate for bone substitution: Synthesis and properties. *Acta Biomaterialia* **2020**, *113*, 23–41.
7. Lu, H. ; Zhou, Y. ; Ma, Y.; Xiao, L. ; Ji, W. ; Zhang, Y. & Wang, X. (2021). Current application of beta-tricalcium phosphate in bone repair and its mechanism to regulate osteogenesis. *Frontiers in Materials* **2021**, *8*, 698915.
8. Liu, B.; & Lun, D. X. (2012). Current application of β-tricalcium phosphate composites in orthopaedics. *Orthopaedic Surgery* **2012**, *4*(3), 139–144.
9. Zhang, Q. ; Zhou, J.; Zhi, P.; Liu, L.; Liu, C.; Fang, A. & Zhang, Q. (2023). 3D printing method for bone tissue engineering scaffold. *Medicine in Novel Technology and Devices* **2023**, *17*, 100205.
10. Ma, H.; Feng, C.; Chang, J. & Wu, C. (2018). 3D-printed bioceramic scaffolds: From bone tissue engineering to tumor therapy. *Acta Biomaterialia* **2018**, *79*, 37–59.
11. Shao, H.; Sun, M.; Zhang, F.; Liu, A.; He, Y.; Fu, J. & Gou, Z. (2018). Custom repair of mandibular bone defects with 3D printed bioceramic scaffolds. *Journal of Dental Research* **2018**, *97*(1), 68–76.
12. Qin, H.; Wei, Y.; Han, J.; Jiang, X.; Yang, X.; Wu, Y. & Chen, L. (2022). 3D printed bioceramic scaffolds: Adjusting pore dimension is beneficial for mandibular bone defects repair. *Journal of Tissue Engineering and Regenerative Medicine* **2022**, *16*(4), 409–421.
13. Cheng, Y. J.; Wu, T. H.; Tseng, Y. S. & Chen, W. F. (2024). Development of hybrid 3D printing approach for fabrication of high-strength hydroxyapatite bioscaffold using FDM and DLP techniques. *Biofabrication* **2024**, *16*(2), 025003.
14. Chen, P.; Liu, L.; Pan, J.; Mei, J.; Li, C. & Zheng, Y. (2019). Biomimetic composite scaffold of hydroxyapatite/gelatin-chitosan core-shell nanofibers for bone tissue engineering. *Materials Science and Engineering*: *C* **2019**, *97*, 325–335.
15. Song, P.; Zhou, C.; Fan, H.; Zhang, B.; Pei, X.; Fan, Y. & Zhang, X. (2018). Novel 3D porous biocomposite scaffolds fabricated by fused deposition modeling and gas foaming combined technology. *Composites Part B: Engineering* **2018**, *152*, 151–159.
16. Januariyasa, I. K. & Yusuf, Y. (2020). Porous carbonated hydroxyapatite-based scaffold using simple gas foaming method. *Journal of Asian Ceramic Societies* **2020**, *8*(3), 634–641.

17. Salehi, M.; Bastami, F.; Rezai Rad, M.; Nokhbatolfoghahaei, H.; Paknejad, Z.; Nazeman, P. & Khojasteh, A. (2021). Investigation of cell-free poly lactic acid/nanoclay scaffolds prepared via thermally induced phase separation technique containing hydroxyapatite nanocarriers of erythropoietin for bone tissue engineering applications. *Polymers for Advanced Technologies* **2021**, *32*(2), 670–680.
18. Kordjamshidi, A.; Saber-Samandari, S.; Nejad, M. G. & Khandan, A. (2019). Preparation of novel porous calcium silicate scaffold loaded by celecoxib drug using freeze drying technique: Fabrication, characterization and simulation. *Ceramics International* **2019**, *45*(11), 14126–14135.
19. Cao, H. & Kuboyama, N. (2010). A biodegradable porous composite scaffold of PGA/β-TCP for bone tissue engineering. *Bone* **2010**, *46*(2), 386–395.
20. Kokubo, T. & Takadama, H. (2006). How useful is SBF in predicting in vivo bone bioactivity? *Biomaterials* **2006**, *27*(15), 2907–2915.
21. Gibson, L. J. (1985). The mechanical behaviour of cancellous bone. *Journal of Biomechanics* **1985**, *18*(5), 317–328.

Publisher's Note: IIKII stays neutral with regard to jurisdictional claims in published maps and institutional affiliations.

© 2024 The Author(s). Published with license by IIKII, Singapore. This is an Open Access article distributed under the terms of the Creative Commons Attribution License (CC BY), which permits unrestricted use, distribution, and reproduction in any medium, provided the original author and source are credited.